James P. Ormsby
Bruce J. Blanchard
Hydrological Sciences Branch
NASA/Goddard Space Flight Center
Greenbelt, MD 20771
Andrew J. Blanchard
Remote Sensing Center
Texas A&M University
College Station, TX 77843

Detection of Lowland Flooding Using Active Microwave Systems

Factors which have a greater effect on response than the incidence angle are the look direction and the presence of moisture on the vegetation at the time the data are acquired.

Introduction

Radar imaging has been recognized as a valuable tool for geologic reconnaissance. As the radar systems with longer wavelengths (>3 cm) became a reality, other land applications began to seem feasible. At the present state of radar system development it is evident that interpretation of data from radar images can be a valuable classification aid for applications in water resources (Benton *et al.*, 1983).

There are several characteristics of microwave systems, and, in particular, active systems such as imaging radar, that make the systems appealing to hydrologists. First, the longer wavelengths can penetrate through clouds and most other atmospheric constituents. Second, they provide their own illumination; thus, they can operate day or night equally well. Third, the longer wavelengths can penetrate to some extent into a volume of vegetation or soils. In addition, the systems can be designed to provide excellent ground resolution even when operating from spacecraft (e.g., Seasat SAR < 25 m, SIR-A 40 m).

Radar images do present some problems to the interpreter who is accustomed to photographic or visible/infrared images. The radar is sensing a set of surface characteristics which have little influence on visible/infrared systems. Radar is primarily sensitive to geometric or roughness features of the terrain and to a lesser extent the dielectric properties of the soil or vegetation (Lillesand and Kiefer, 1979). The image observer should be aware that response from geometric or roughness features is influenced by the element dimensions, orientation in respect to the incident energy, distribution of the elements within the area, the dielectric of the surface of the

Abstract: *Radar systems are becoming increasingly important as a means of providing new insight into hydrologic phenomena. L-band 23-cm wavelength data acquired by the Seasat-A radar imaging system and the Shuttle Imaging-Radar-A (SIR-A), over two wildlife refuges, have indicated the capability of detecting flooding under forest canopies. While others have reported on this capability of radar systems, there has been no previous opportunity to quantify the increase in microwave scattering brought about by the reflection and re-scattering phenomena. In this study, non-imaging airborne scatterometer data were available to corroborate the Seasat-A data. In these cases, the difference in scattering coefficient from beneath flooded and non-flooded forest canopies ranges from approximately 3dB to 6dB. In addition to the L-band radar, aircraft X-band and C-band radar images were available over the same, or similar, areas. The SIR-A data were optically processed and can only be compared to the Seasat-A and scatterometer data in a qualitative sense; however, these data illustrate that the radar response to flooding under forest canopy is not diminished by increasing the incidence angle.*

Photogrammetric Engineering and Remote Sensing,
Vol. 51, No. 3, March 1985, pp. 317-328.

0099-1112/85/5103-0317802.25/0

element, the dielectric of the material within the element, and the wavelength of the radar. All of these factors effect both the amount and direction of scattering and ultimately determine the amount of energy redirected back to the radar.

Detectable features in radar images caused by differences in dielectric properties are usually associated with the water content of either soils or vegetation. Because most natural soils and dry organics have a very low (3 to 8) dielectric constant, while water has a high dielectric constant (≈80), mixtures of these materials can produce a wide range of values. Dielectric effects on the radar image are comingled with the effects from roughness and/or vegetation. On most natural terrain the effects from roughness and vegetation are dominant over the dielectric effects. One notable exception to this generality is the case where vegetation or rough surfaces are coated with water. In this instance, the radar return increases dramatically. This increase comes both from increased scattering efficiency and the dielectric of water. The vegetation in this circumstance responds similarly to a very rough surface on an open body of water.

Another peculiarity of radar images of particular interest to hydrologists is the dramatic increase in return from certain flooded vegetated areas. In early radar imagery, typically shorter wavelengths usually less than 3 cm, high returns from vegetated areas were seen only where relatively short vegetation such as grasses were flooded. More recently, with the development of radars such as the Seasat SAR with a 23.5-cm wavelength, the same response is seen in flooded forest. Waite *et al.* (1981) described observations of this type of response in forested areas of Arkansas and other southern states while Krohn *et al.* (1983) describes the situation in eastern Maryland and Virginia using the Seasat SAR imagery.

Questions still remain concerning the capability of radar for the detection of flooding under vegetation. First, what is the magnitude of the increase in backscatter due to flooding under vegetation? Is this response influenced by plant species, i.e., in the case of L-band imagery is the response similar for different species of trees? Is the increased response over flooded forest dependent on the incidence angle of the radar beam? Finally, what is the response from different wavelengths?

Approach

When the studies reported in this paper were initiated in 1976, the intent was to define the magnitude of the effects on radar data caused by flood waters under vegetation. The approach at the time was to merely fly the NASA L-band scatterometers over a target of opportunity where a flooded alluvial plain had a variety of vegetation standing over the water. The site was to be in Texas in order that repeat coverage could be obtained after recession of the flood waters. Flooding occurred along a major reach of the Navasota River near College Station, Texas on 20 April 1977, and a flight line 20 kilometres in length was flown parallel to the river. Repeat coverage with the same system was acquired the following year on 4 May 1978. At that time it was known that some land areas would be imaged with the Seasat Synthetic Aperture Radar (SAR) within the continental United States. Coverage was requested for some coastal areas in order to substantiate the L-band scatterometer data with L-band SAR data.

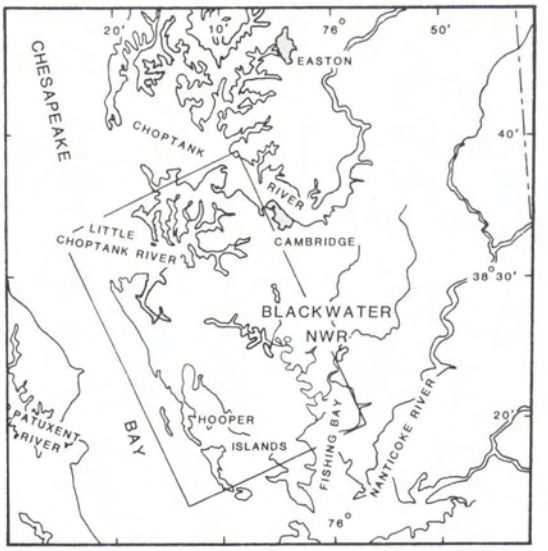

FIG. 1. Location of the Blackwater National Wildlife Refuge (NWR) with respect to the SAR and MSS data.

The Seasat SAR acquired repeated coverage over flooded areas in and near the Blackwater Natural Wildlife Refuge (NWR) on the eastern shore of the Chesapeake Bay in Maryland (Figure 1). These images were collected on three-day intervals during late September in 1978 from ascending orbits. During this same period one ascending and one descending orbit provided images of an area near the Croatan National Forest in North Carolina (Figure 2). Cursory examination of these images led to attempts to collect other imagery over these two coastal areas.

The Shuttle Imaging Radar (SIR-A) imaged the North Carolina site on 13 November 1981 and a portion of the same area was imaged the same day with an aircraft-mounted X-band system. Later the same month, a C-band imaging radar was flown over a small portion of the Maryland site. Acquisition of this variety of imagery provided an opportunity to examine the effects of two depression angles with L-band systems, the effects of climatic differences on the different dates, and the effects of using different frequencies.

Documentation of ground conditions was done immediately after collection of the scatterometer

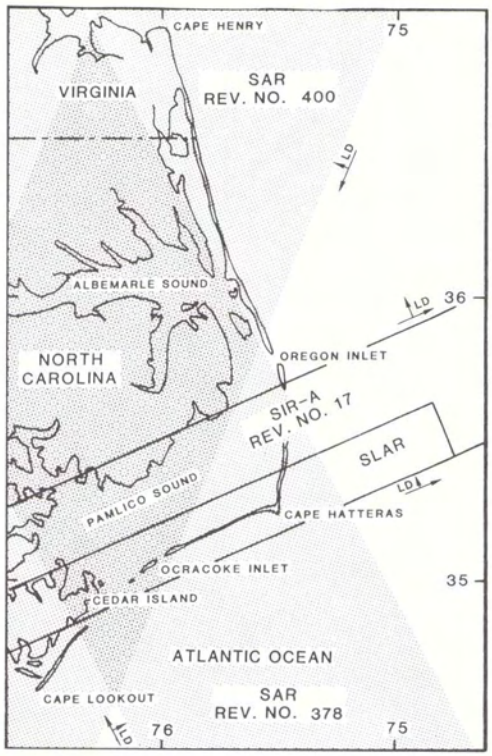

FIG. 2. Location of Cedar Island with respect to the Seasat SAR, SIR-A and SLAR data taken.

data flights, and within six weeks after the Seasat SAR coverage for the Maryland site. Ground data for the remaining imagery were collected over an extended period after the images were acquired.

The scatterometers were provided with a calibration and the Seasat SAR optically processed data were pseudo-calibrated; these were the only data treated as quantitative. The remaining radar images, photographs, and Landsat data over these sites must be considered as qualitative. Our approach has been to interpret the images with the characteristics of radar in mind in order to accomplish the remainder of our objectives.

SITE DESCRIPTIONS

The Navasota River site in Texas is a flat alluvial plain averaging approximately 5 km in width which is subject to frequent flooding. The land use is, therefore, primarily brushy rangeland with intermittent forested areas. Three forested areas along the flight line used in this study have a mixture of oak species with some sycamore, pecan, and elm scattered throughout the stand. The trees ranged in height from 20 to 30 metres and were leafed out at the time of both flights. Local low level flights over these areas and ground surveys were made at the time of the flooding to determine limits of the flood waters under the vegetation.

The Blackwater NWR is a flat low lying marsh and wooded area in Dorchester County, Maryland, south of Cambridge. The vegetation consists of marsh grass, small shrubs, and considerable standing water. Pine and deciduous timber stands surround the marsh and become flooded at times of high tide or as a result of entrapment of water in swales.

Three areas near the NWR were chosen for closer investigation. Several smaller subsites were chosen within these three areas and are indicated on Figure 3. Vegetation cover, climatic conditions, and water conditions were documented and photographed during field trips to these areas. Area 1, within the refuge, consists mainly of coniferous trees. The second area lies east of the refuge and is mainly deciduous (ash) trees. The third area, north of area two, is mixed deciduous and coniferous. Within these three areas, smaller sites were picked. Subsite A in area one is predominantly pine, Subsite B is 60 percent pine and 40 percent deciduous (ash), and Subsites C and D consist of 60 percent pine with a mixture of deciduous trees and marsh. Within the second area, Subsite E is 95 percent short (12 metres) ash. Subsite F is 80 percent tall pine and ~20 percent short deciduous trees. Subsite G is almost entirely short deciduous trees. Subsite H is a half and half mix of pine and deciduous trees. The third area consists of Subsite I which is mainly deciduous and Subsite J which is mixed ash and pine. Subsites A, C, E, G, and I were inundated with standing water at the time of the Seasat SAR overflights.

Cedar Island NWR is located at the end of a peninsula on the North Carolina Atlantic coast. To the north it is bounded by West Bay and on the Atlantic Ocean by Core Sound. The refuge area consists of irregularly flooded saltmarsh and over 2000 acres of woodland. The dominant saltmarsh vegetation includes black needlebrush (Juncus spp.), three species of cord grass (Spartina spp.), salt grass (Distichlis spicata), and switch grass. The woodland areas are dominated by loblolly (Pinus taeda), longleaf (P. palustris), and pond pines (P. serotina). Live oak (Quercus virginiana) can be found on the upland sites (Dept. of Interior, 1980). Cedar Island itself is entirely forest, although the land surfaces are only slightly above sea level and portions of the island are poorly drained. The island is separated from the mainland by a large marsh land area, and another large grassy marsh land is located directly west across the bay.

DATA

The variety of sensors used in this study are listed along with some of their characteristics in Table 1. Data from these sensors will be discussed by site and chronological order that the data were collected at each site.

The scatterometer data are provided in a digital

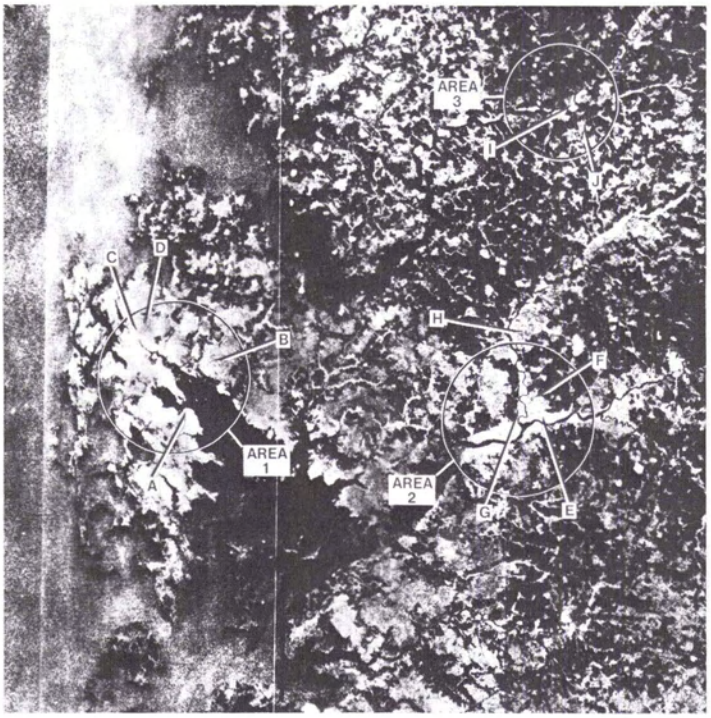

FIG. 3. Blackwater—Test areas and subsites, SAR image.

form representing the scattering coefficient (σ^0 in dB), the angle off nadir, and the time of the observation. In this analysis only the 20° off nadir look angle was used in order that the data would be comparable to the Seasat SAR data. The scatterometer had been flown over the Navasota River site under flooded and non-flooded conditions on 20 April 1977 and 4 May 1978, respectively (Blanchard *et al.*, 1981). Time intervals were selected for three flooded forest sectors of the first flight line and average scattering coefficients were calculated for those sectors. The same sectors for the second (dry) flight line were used to determine the scattering coefficients for dry conditions. Upland forest areas that were not flooded on the 1977 flight line produced averaged returns equal to the 1978 return; thus, the flight lines are comparable in a quantitative sense. Differences in the scattering coefficients for flooded and non-flooded conditions are shown in Table 2.

Over the Maryland-Blackwater NWR site, Seasat-SAR data were collected on 29 August, 22 September (orbit #1253), 25 September (orbit #1296), 28 September (orbit #1339), 4 October (orbit #1425), and 7 October in 1978. Although the SAR data processing is available in both optical and digital forms, only the optically processed data were used. In this type a pseudo-calibration technique (Thompson, 1979) was available to derive scattering coefficients from the density of the imagery. Using this technique, estimated scattering coefficients were found for the subsites on the four sets of images indicated in Table 3. The differences in the coefficients for adjacent flooded and non-flooded pairs of subsites were then calculated. There were inadequate ground data to define the actual limits of flooding for 29 August and 7 October and no opportunity on the Blackwater site to have a totally non-flooded condition.

An attempt was made to acquire C-band radar imagery on 30 November 1981, over a portion of the Blackwater site; however, due to navigation problems, Hooper Island south and west from the refuge was imaged. The image was optically processed and is not provided with any means of calibration. Other remotely sensed data over the Blackwater site included color infrared photography (Mission 103, 15 September 1969) and Landsat-2 digital imagery (ID#22362-15041, 11 July 1981).

Ground conditions at this site were documented on a series of field trips beginning in November 1978 and continuing through 1983. Aerial photographs were used to determine precise location of the subsites. Vegetation types, flooding conditions, climatic conditions, and tides were documented for each date that radar images were taken.

The Cedar Island site in North Carolina was imaged with the Seasat SAR on two orbits (Orbit 378, 23 July 1978 and Orbit 400, 25 July 1978). Orbit 378 was ascending; thus, the radar was looking north of east while orbit 400 was descending and looking north of west. These data were acquired only in optically processed images and no attempt was made to quantify the radar return.

On 13 November, 1981, the SIR-A imaged the

TABLE 1. COMPARISON OF THE SENSOR CHARACTERISTICS FOR THE VARIOUS DATA USED

Characteristics	SEASAT SAR	Shuttle SIR-A	Aircraft X-Band	Aircraft C-Band	Aircraft L-Band Scat
Wavelength (CM)	23.5	23.5	3	5.45	18.75
Frequency (GHz)	1.28	1.28	10	5.5	1.6
Depression Angle	70°	40°	16-29°	60-80°	30-85°
Altitude	800KM	257 × 267 KM	1.18KM	18.29KM	.30KM
Resolution	25M	40M	31-34M	15M	50M
Inclination	108°	38°	NA	NA	NA
Swath Width	100KM	50KM	25KM	7.4KM	NA
Processing	Optical and Digital	Optical	Optical	Optical	Digital

Cedar Island site looking west of north and the X-band radar mounted in an aircraft imaged a portion of the SIR-A image area while looking in the same direction. Data from these two systems are also optically processed and can only be used in a qualitative sense. The complete set of radar images over this site provide three L-band look directions, three different dates, two off-nadir look angles for L-band and two frequencies on the same date. Landsat digital imagery (ID#22523-15010, 9 December 1981) collected near the time of the SIR-A radar imagery was also available.

A field trip was made to this site in 1982 to collect ground data and verify the vegetation types. Tidal information was obtained from the National Ocean Survey. The closest station to the study area was located at Beaufort, North Carolina (Duke Marine Laboratory, #8656483). On 13 November 1981, at approximately 9 A.M. the highest tide (7.05 feet) of the month occurred (see Table 4). This is 3.74 feet above mean sea level (MSL) and 2.28 feet above the 19-year Tidal Epoch mean high water (NOAA/NOS, 1981).

On 13 November 1981, the day of the shuttle overpass, a high pressure system centered over New York state (Figure 4) coupled with a low off the North Carolina coast produced winds in excess of 24 kts (NOAA/LCD, 1981). At the refuge weather station, winds were recorded between 40 and 45 miles per hour (personal communication, H. Brohawn, 1982). Wave action coupled with the high tide would have been sufficient to cause flooding of the lowland areas within the refuge, as well as along the rivers and streams.

Hourly precipitation data (NOAA, 1981) for North Carolina indicates 0.63 inch of rain fell at Cape Hatteras, northeast of Cedar Island, from 10 to 12 November 1981. At Morehead City, west of Cedar Island, 0.4 inch of rain fell for the same period. There was, however, no rainfall within a 24 hour period prior to the overpass of SIR-A.

DISCUSSION

Contrasts in the L-band radar return between flooded forest and non-flooded forest are evident in the image of the Blackwater NWR (Figure 3). Comparison of these differences in a quantitative sense are shown in Tables 2 and 3. Although three subsite pairs on some images could not be estimated due to saturation of the film, the values in Table 3 are consistent with the difference in return from flooded and non-flooded scatterometer data shown in Table 2. During this period no precipitation occurred (NOAA, 1978); thus, all variation was due to surface roughness as well as signal enhancement due to the standing water beneath the canopy. The slight difference in specie mix, with the exception of pair C-D, may have played a part in the enhancement as discussed by Krohn *et al.* (1983) Krohn *et al.* (1981), and Wu (1983), but because the original intent was to detect and delineate flooded forest,

TABLE 2. 1.6 GHz SCATTEROMETER DATA NEAR THE NAVASOTA RIVER

Site	Backscatter Difference (ΔdB)
A	4
B	3
C	3.5
Data Obtained Near Navasota River in Texas	
First Flight	20 April 1977 Flooded
Second Flight	4 May 1978 Non-flooded

this was not considered in the analysis. Overall, these values show agreement between the sensors, and in all instances the values are positive, thus showing an increase of approximately 3 to 6 dB can be expected from flooding under forest cover regardless of specie mix.

The Seasat SAR image of the Blackwater NWR is repeated in Plate 1 to illustrate how the radar image contrasts with Landsat MSS imagery. Flooded timber areas are detectable in the SAR image along the Blackwater River and other shore areas adjacent to the marshland. Plate 2 shows a typical scene in the flooded forest areas that produce the brightest return in the Blackwater NWR. These areas are not detectable in the Landsat image; however, the marshlands that had smaller vegetation standing above water are detectable in the Landsat image and not in the SAR image. On the other hand, the separation of open land from open water bodies is clear in the Landsat image and, in many instances, difficult to detect in the SAR image. These observations substantiate the premise that a combination of these two types of data will be of considerable value in water resources investigations.

A greater variety of imagery was available over the Cedar Island site. Plate 3 offers an opportunity to compare both X-band aircraft radar imagery (provided by Michael Mattie, U.S. Army Topographic Labs) with L-band SIR-A imagery as well as Landsat imagery. The two radar images were collected on the same day, 13 November, and because there was no recorded rain that day, the leaves on vegetation should have been dry. The straight bright line in the L-Band SIR-A is caused by a power line oriented parallel to the flight line and normal to the look direction of the radar. Cedar Island itself is quite well defined by the bright return on the right side of the L-Band SIR-A. Note that the northwest tip of the island is black, indicating a low return while it is well defined in the X-band image. Due to the combination of a high tide and east wind, there was water under both the forest on Cedar Island and the shorter marshlands vegetation. The L-band image shows the same high response from flooded forest and low response from flooded marsh vegetation that was evident at the Blackwater NWR site.

The X-band image shows an extremely high return from the low elevation marshland with moderate return from the higher marsh and the forested areas. Note that there is no discrimination in X-band between the forest and non-flooded marsh while these vegetation classes are easily discriminated in the Landsat and the L-band images.

The forested area, predominantly conifers, in the left portion of these images is for the most part not subject to flooding. The vegetation in the marsh areas consists of black needlerush, three species of cord grass, salt grass, and switch grass. These plants do not impede the longer L-band wavelength energy. Instead, they act to calm the water surface which reflects the incoming energy away from the sensor. The brighter response, on the other hand, coming from the wooded area on the eastern end of the peninsula for the SIR-A data (Plate 3c) is the result of volume scattering within the canopy followed by reflection or a portion of the scattered energy from the water surface and subsequent rescattering.

The X-band energy undergoes similar scattering, partial reflection, and rescattering in the flooded marshland plants. This shorter wavelength does not penetrate the forest canopy enough to allow any rescattering from reflection. There is an obvious correlation between the radar wavelength and the geometry and or dimension of the vegetation in contrast to the reflectance that is observed by the Landsat MSS. These observations lead one to conclude that not only can flood boundaries be detected beneath a forest canopy with L-band radar, but also that a combination multifrequency radar with a visible-near infrared data system such as Landsat would enhance land use classification.

Figure 5 shows three different L-band images taken over the Cedar Island site where there are differences in look direction and incidence angle.

TABLE 3. BACKSCATTER CROSS SECTION DIFFERENCES OVER THE BLACKWATER NWR

Orbit No. Subsite Pairs	Δ1(dB) A-B	Δ2(dB) C-D	Δ3(dB) E-F	Δ4(dB) G-H	Δ5(dB) I-J
1253	4.1	4.3	6.4	2.5	4.0
1296	3.8	3.9	*	*	4.8
1339	3.9	3.5	*	*	6.3
1425	5.6	3.0	*	*	*

* Film saturated.

TABLE 4. TABLE SHOWING THE HOURLY TIDES IN FEET FOR THE BEAUFORT DUKE MARINE LAB, N.C., #8656483.
TIME OF MAXIMUM TIDE HEIGHT UNDERLINED

8656483 Beaufort Duke Marine Lab NC Nov. 1981	0/12	1/13	2/14	3/15	4/16	5/17	6/18	7/19	8/20	9/21	10/22	File Copy 11/23
					National Ocean Surveys (NOAA) Tides, Hourly Heights (Feet) TM 075W M							
1	4.24	3.70	3.18	2.75	2.58	2.77	3.25	3.80	4.37	5.00	5.36	5.44
	5.03	4.38	3.84	3.29	2.92	2.86	2.95	3.25	3.68	4.12	4.54	4.66
2	4.40	3.86	3.35	2.81	2.54	2.50	2.79	3.31	3.83	4.40	4.91	5.21
	5.15	4.62	3.96	3.35	2.91	2.62	2.65	2.72	3.06	3.50	3.91	4.24
3	4.26	3.93	3.38	2.88	2.49	2.26	2.30	2.61	3.05	3.55	4.15	4.60
	4.79	4.65	4.04	3.48	2.99	2.58	2.33	2.30	2.46	2.89	3.42	3.82
4	4.06	4.01	3.56	3.18	2.73	2.38	2.15	2.19	2.57	3.07	3.66	4.18
	4.54	4.64	4.38	3.86	3.42	2.95	2.52	2.27	2.16	2.41	2.98	3.47
5	3.89	4.08	3.99	3.60	3.15	2.72	2.37	2.14	2.23	2.61	3.11	3.63
	4.12	4.45	4.51	4.41	3.99	3.54	2.89	2.44	2.28	2.29	2.48	3.24
6	3.78	4.00	4.23	4.15	3.93	3.39	3.03	2.52	2.24	2.18	2.57	3.25
	3.90	4.38	4.82	4.99	4.90	4.43	3.78	3.12	2.59	2.34	2.48	2.76
7	3.21	3.58	4.19	4.57	4.60	4.46	3.90	3.28	2.63	2.37	2.35	2.83
	3.43	3.90	4.58	4.95	5.10	4.90	4.30	3.59	2.85	2.33	2.09	2.33
8	2.86	3.61	4.20	4.68	4.97	4.90	4.35	3.71	3.11	2.50	2.16	2.10
	2.60	3.26	3.82	4.49	4.90	5.07	4.76	3.92	3.19	2.45	1.92	1.72
9	2.06	2.82	3.57	4.24	4.83	5.11	5.05	4.43	3.69	2.96	2.23	1.82
	1.83	2.32	3.18	3.91	4.63	5.04	5.11	4.54	3.74	2.99	2.13	1.61
10	1.52	2.18	3.02	3.82	4.64	5.23	5.54	5.45	4.60	3.72	2.92	2.18
	1.78	1.80	2.40	3.25	4.09	4.75	5.16	5.12	4.48	3.64	2.82	2.03
11	1.56	1.66	2.29	3.36	4.26	5.16	5.73	6.03	5.89	5.13	4.10	3.22
	2.43	2.08	2.25	2.77	3.77	4.49	5.07	5.54	5.63	4.82	3.98	3.13
12	2.35	1.93	1.88	2.70	3.64	4.55	5.48	6.23	6.59	6.35	5.30	4.50
	3.65	2.88	2.47	2.40	2.89	3.85	4.76	5.50	5.84	5.81	5.09	4.39
13	3.56	2.91	2.55	2.60	3.36	4.34	5.31	6.28	6.92	7.05	6.62	5.58
	4.79	3.92	3.24	2.85	2.84	3.41	4.30	5.13	5.75	6.11	5.90	5.16
14	4.41	3.69	3.06	2.73	2.88	3.64	4.60	5.51	6.41	6.92	6.92	6.30
	5.40	4.68	3.86	3.29	3.02	3.14	3.81	4.63	5.31	5.84	6.00	5.73
15	5.00	4.30	3.60	3.06	2.79	2.99	3.85	4.75	5.62	6.38	6.79	6.74
	6.16	5.30	4.60	3.92	3.41	3.21	3.30	3.90	4.65	5.33	5.78	5.89
16	5.59	4.86	4.21	3.57	3.14	3.00	3.28	4.05	4.83	5.64	6.33	6.66
	6.57	5.98	5.18	4.44	3.89	3.47	3.25	3.32	3.78	4.44	5.11	5.46
17	5.50	5.24	4.60	4.34	3.65	3.25	3.00	3.35	3.82	4.65	5.27	5.77
	5.99	5.80	5.37	4.65	3.99	3.34	2.78	2.59	2.87	3.50	4.25	4.67
18	4.89	4.76	4.59	4.33	3.82	3.16	2.64	2.47	2.57	3.20	3.96	4.58
	5.09	5.31	5.29	4.94	4.37	3.81	3.28	2.68	2.47	2.60	3.26	3.90
19	4.47	4.81	4.87	4.62	4.16	3.61	3.04	2.59	2.41	2.59	3.18	3.80
	4.38	4.86	5.11	5.05	4.62	4.13	3.49	2.89	2.47	2.30	2.61	3.21
20	3.68	4.23	4.64	4.86	4.75	4.26	3.76	3.25	2.77	2.58	2.71	3.22
	3.69	4.42	4.67	4.89	4.97	4.94	4.26	3.41	2.72	2.12	1.68	1.86
21	2.66	3.33	3.76	4.23	4.49	4.28	3.82	3.31	2.71	2.16	1.76	1.96
	2.55	3.19	3.76	4.06	4.34	4.41	4.07	3.38	2.71	2.11	1.68	1.62
22	2.23	2.92	3.56	4.15	4.58	4.78	4.67	4.06	3.39	2.70	2.19	1.93
	2.18	2.69	3.31	3.80	4.25	4.51	4.45	3.84	3.17	2.49	1.93	1.66
23	1.73	2.26	2.96	3.62	4.20	4.66	4.80	4.43	3.74	3.10	2.51	1.95
	1.77	2.00	2.54	3.25	3.82	4.25	4.41	4.18	3.56	2.96	2.34	1.89

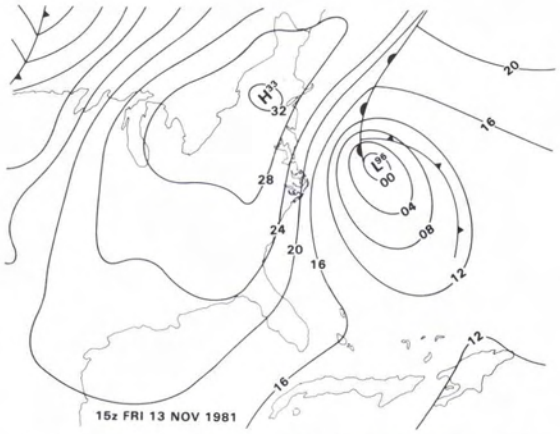

FIG. 4. Simplified weather map showing location of systems affecting weather at Cedar Island.

Image A is from an ascending orbit (No. 378) of Seasat taken on 23 July 1978, while Image B is from a descending orbit (No. 400) that was taken on 25 July 1978, and Image C is from the SIR-A overpass taken on 13 November 1981. These three scenes provide an opportunity to examine the radar return from the same vegetation using a single frequency (L-band) at different look directions and incidence angles and under different climatic conditions. The Seasat SAR operated at a 20 degree incidence angle and the SIR-A operated at 50 degrees. In both sets of imagery there was enhanced return from flooded forest areas; thus, observations of flood boundaries do not appear to be influenced significantly by the difference in incidence angles.

The look directions shown in Figure 5 are different for each image, and there is one example of effects from look direction in these images. In the SIR-A image, the look direction was perpendicular to a portion of the power line across the central area of the marsh which produced the bright linear feature. Other portions of the power line extending from both forested areas into the marsh were nearly perpendicular to the look direction of the Seasat SAR, image B, and produced detectable linear features. Where none of the power lines were near perpendicular to the look direction, image A, there is no indication that the power line exists. These observations are consistent with results previously published by Waite *et al.* (1980) and Blanchard and Chang (1983).

Differences in the three images in Figure 5 illustrate primarily the climatic effects on radar images. Image A, was taken when no previous rainfall had occurred within 48 hours while image B was taken 2 days later at 7:05 P.M. (0005 GMT). Cape Hatteras recorded almost an inch (0.92) of precipitation during the hour of the 25 July pass. Morehead City, southwest of Cedar Island, recorded 0.80 inch prior to 9 P.M. Thus, as indicated by the increased response from both forest and marsh grasses, rainfall had wet the vegetation surfaces prior to imaging. The SIR-A image, on the other hand, had not had rainfall in the previous 24 hours but portions of the lower elevation were flooded. Note that in the SIR-A image the higher elevations in the forest on the mainland have a reduced return and the marsh grasses between the mainland and Cedar Island have ever less return. There is little or no scattering of the L-band energy by the marshland vegetation unless the surfaces of the leaves are wet.

The scattering phenomena of the radar energy is illustrated in an idealized fashion in Figure 6. Using the X- and L-band wavelengths, one can readily distinguish the shorter marsh grasses from the taller forest land vegetation. In addition, those areas where flooded vegetation exists can be easily identified. The presence or absence of standing water becomes a key factor in the scattering effect when

FIG. 5. Comparison of L-band radar response over Cedar Island from different look angles and directions.

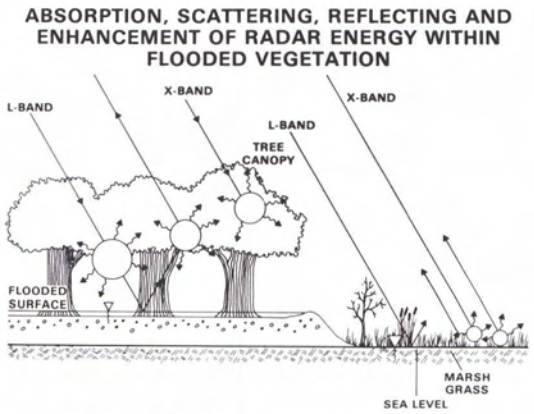

FIG. 6. Effect of flooded vegetation on X- and L-band radars.

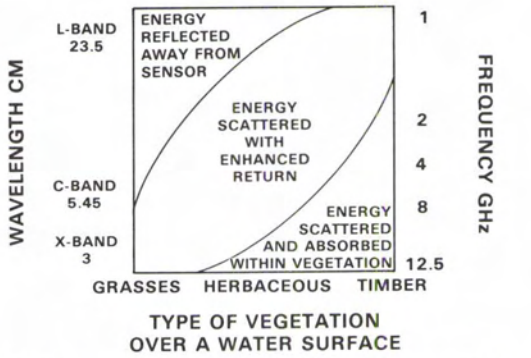

FIG. 7. Diagram showing the relative radar responses for different wavelengths and vegetation conditions.

the wavelength is synchronized with the geometry or dimensions of the vegetation.

The generalized response and relative effects that various types of flooded vegetation produce when subjected to different radar frequencies is illustrated in Figure 7. Now, to illustrate that these generalizations may be misleading, we present in Plate 4 the one example of C-band imagery available. Middle Hooper Island shown in this figure was imaged when the vegetation was dry, and the color infrared image of the island clearly shows the loblolly pine trees as a dark red while the dark green areas are brushy tall marsh grasses. Note that, in the C-band radar image, the trees produce a low response, indicating that energy at this wavelength is absorbed by the vegetation. This is contrary to results at other frequencies and makes one wonder if other frequencies would respond the same way over selected vegetation. Obviously, much more documented imagery must be collected at different incidence angles to resolve the numerous questions posed by this result.

CONCLUSIONS

What is the magnitude of the increase in backscatter due to flooding under vegetation? As stated earlier, for the L-band radar, the quantitative change in response between flooded and nonflooded conditions ranged from 3 to 6dB (see Tables 2 and 3). This indicates that it is feasible to detect flood conditions beneath a forest canopy as well as to better define the land/water boundary, which for the most part cannot be seen in or interpreted well from visible or near-IR imagery.

The improved capability to detect the land/water boundary under varying vegetative conditions using multispectral visible, near infrared, and microwave imagery provides, through repeated observations, improved floodplain delineation. Using detailed topographic maps, the flood extent can be mapped, providing water resources management with information needed to assess flood damage and extent and project to the 20-, 50-, and 100-year flood.

What influence do plant specie and wavelength have on response? The response depends upon wavelength, plant volume or height, geometry of the vegetation, and the presence or absence of standing water within the vegetation. The L-band response from the shorter vegetation species growing in water, such as marsh grass, was minimal, if any, when the ground surface was flooded, but can become significant if leaves are wet from rainfall (Figure 5B). With increased height and vegetation volume, the amount of scattering and enhancement increases when the ground if flooded (Figure 5C). For the shorter X-band wavelength the incoming energy is scattered within the canopy with some returning to the antenna. In the case of the short grasses, some of this energy is reflected from the water surface and then subsequently rescattered back to the receiver (Plate 3A), producing a brighter return.

The taller vegetation also scatters the incident X-band energy, but due to the shorter wavelength there is less penetration and, thus, no enhancement from the water surface below (Plate 3A compared with Plate 3C). A single high frequency radar (shorter wavelength) will not provide the discrimination needed between vegetation density and height with or without flooding when compared to lower frequency (longer wavelength) L-band radar.

What effect does incidence angle have on response? The difference in response due to the presence of flooding does not appear to be dependent on the incidence angle of the sensor. Similar responses were observed (enhanced return from flooded timber areas) from the SIR-A (Plate 3 or Figure 5) (50° incidence angle) and Seasat SAR (Plate 1) (20° incidence angle). On the other hand, the observed response from the Middle Hooper Island C-band radar imagery may be the result of the near-nadir incidence angle (10° to 30°). This steep angle plus the shorter wavelength could be producing the "enhanced" response from the shorter vegetation

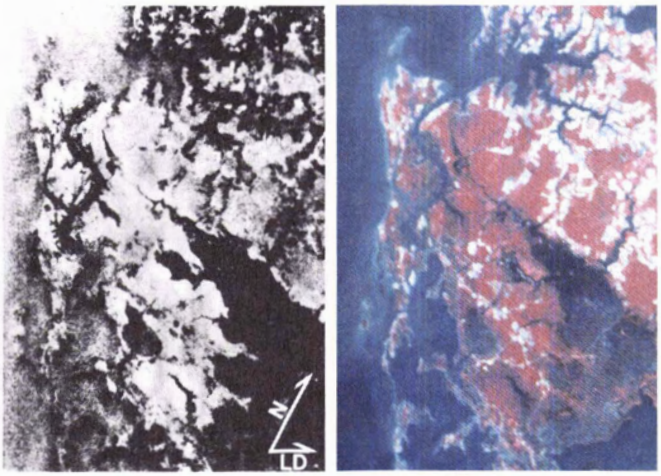

PLATE 1. Comparison of Seasat SAR and Landsat MSS over the Blackwater National Wildlife Refuge.

PLATE 2. Photo showing ground conditions beneath one of the flooded forest areas.

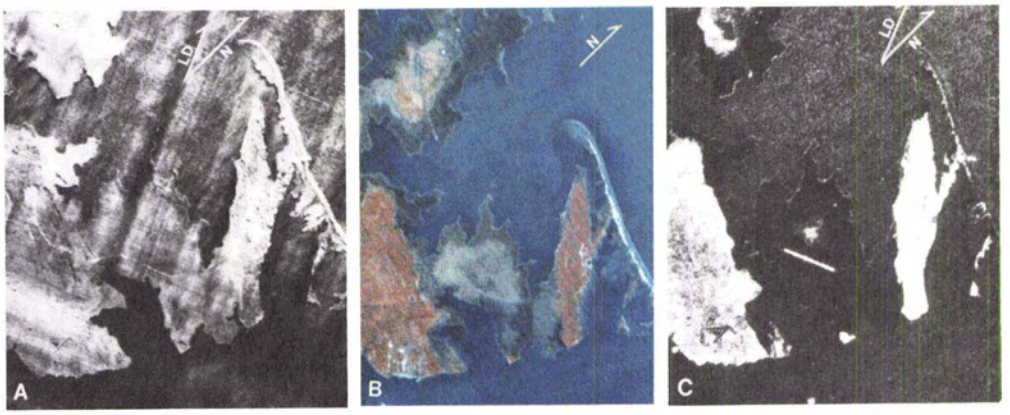

PLATE 3. Comparison of L-band and X-band radar imagery with a Landsat-2 MSS scene over Cedar Island National Wildlife Refuge, N.C.

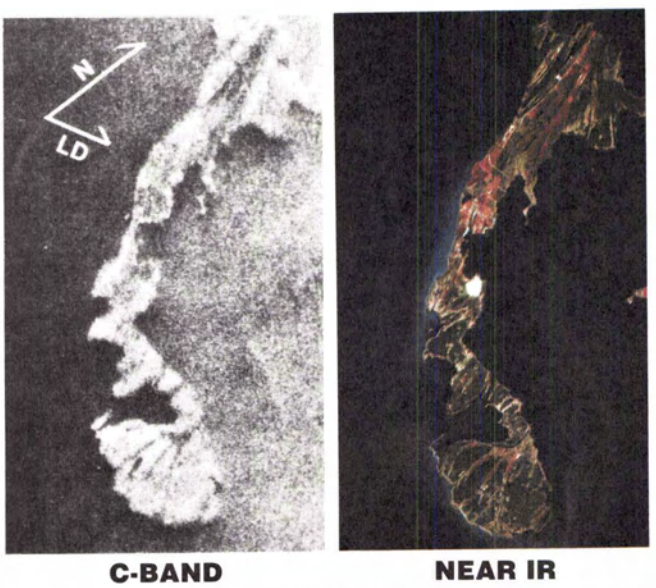

PLATE 4. C-band radar over Middle Hooper Island compared with a color-IR image.

with respect to the taller loblolly pine. Regardless of these observations, factors which have a greater effect on the response are the look direction and the presence of moisture on the vegetation at the time the data are acquired.

The optimum means for obtaining information on wetland extent and defining flood boundaries is through a multispectral approach using visible, near- and/or middle-IR, and well chosen microwave frequencies. One microwave frequency (e.g., L-band), as well as one visible channel (e.g., near-IR 0.8 μm to 1.1 μm or 0.76 μm to 0.90 μm), will not do the job effectively. As was shown, the L-band frequency helps separate the deciduous/coniferous vegetation from the shorter, partially submerged grasses and shrubs. In addition, higher frequency, shorter wavelength C- and X-band radar are needed to further define the relative heights of the shorter vegetation. As depicted on Plate 3, a considerable amount of information can be gleaned from the false color MSS in combination with the shorter wavelength X-band data and the longer wavelength L-band data. The visible data provides insight into vegetation and non-vegetation features as well as soil/crop and land/water contrasts.

Some questions have been answered, but as in any effort involving multiple dates, places, and sensors, slightly different conditions prevail, leaving one with some doubt as to the general validity of the conclusions. Thus, there is a need for further study in which multiwavelength sensors are available on the same platform.

References

Benton, Jr., A. R., A. J. Blanchard, and R. W. Newton, 1983. Multifrequency Radar Interpretation Techniques Applied to the Coastal Zone, ASCM-ASP Fall Convention, Salt Lake City, Utah.

Blanchard, B. J., *et al.*, 1979. "Continuation of the Measurements of Hydrologic Soil-Cover Complex with Airborne Scatterometers," NASA/GSFC, Contract No. NSG 5156, Final Report 3496, Remote Sensing Center, Texas A&M University, College Station, Texas.

———, 1981. *Seasat SAR Response from Water Resources Parameters*, Final Report 3891. USDC-NOAA Contract 78-4332. Remote Sensing Center, Texas A&M University, College Station, Texas.

Blanchard, B. J., and A. T. C. Chang, 1983. Estimation of Soil Moisture from Seasat SAR data, *Water Resources Bulletin*, AWRA, Vol. 19, No. 5.

Elachi, Charles, 1980. Spaceborne Imaging Radar: Geologic and Oceanographic Applications, *Science*, Vol. 209, September 5.

Honeycutt, B., 1979. *Calculation of Range of Detectable σ_o for Seasat-A SAR System*, Interoffice Memorandum 334.5-101, JPL, Pasadena, Calif.

Krohn, M. Dennis, N. M. Milton, and Donald B. Segal, 1983. SEASAT Synthetic Aperture Radar (SAR) Response to Lowland Vegetation Types in Eastern Maryland and Virginia, *Journal of Geophysical Research*, Vol. 88, No. C3, pp. 1937-1952.

Krohn, M. D., N. M. Milton, D. Segal, J. Crowley and A. England, 1981. Seasat L-Band Radar Response to Forest Vegetation in Eastern Virginia, *1981 IEEE International Geoscience and Remote Sensing Symposium Digest*, Washington, D.C.

Lillesand, Thomas M., and Ralph W. Kiefer, 1979. *Remote Sensing and Image Interpretation*, John Wiley and Sons, Inc., New York.

NOAA. *July 1978, Hourly Precipitation Data, North Carolina*, National Climatic Center, Asheville, N.C.

NOAA. *July 1978, Local Climatological Data, North Carolina*, National Climatic Center, Asheville, N.C.

NOAA. *September and October 1978, Hourly Precipitation Data, Maryland and Delaware*, National Climate Center, Asheville, N.C.

NOAA. *November 1981, Hourly Precipitation Data, North Carolina*, North Climatic Center, Asheville, N.C.

NOAA. *November 1981, Local Climatological Data, North Carolina*, National Climatic Center, Asheville, N.C.

NOAA/National Ocean Survey, 1981. *Tidal Information*, Duke Marine Lab. #865-6483, Rockville, Md.

Settle, Mark, and James V. Taranik, 1982. Use of the Space Shuttle for Remote Sensing Research: Recent Results and Future Prospects, *Science*, Vol. 218, No. 4576.

Thompson, T. W., 1980. Personal communication.

U.S. Department of Interior, 1980. Cedar Island National Wildlife Refuge, U.S. Fish and Wildlife Service, Cedar Island, North Carolina.

Waite, W. P., H. C. MacDonald, V. H. Kaupp, and J. S. Demarche, 1981. Wetland Mapping With Imaging Radar, 1981 International Geoscience and Remote Sensing Symposium (IGARSS '81), June 8-10, 1981, Washington, D.C., IEEE Geoscience and Remote Sensing Society.

Waite, W. P., H. C. MacDonald, J. S. Demarcke, and B. H. Corbell, 1980. Look Direction Dependence of Radar Backscatter Cross Section for Agricultural Fields, *Proceedings, Fall Technical Meeting, American Society of Photogrammetry*, Niagara Falls, New York, pp. R-2G-1 to R-2G-14.

Wu, S. T., 1983. Analysis of Synthetic Aperture Radar Data Acquired Over a Variety of Land Cover, *1983 IEEE International Geoscience and Remote Sensing Symposium Digest*, San Francisco, Calif.

(Received 10 March 1984; revised and accepted 30 October 1984)

Errata

The date of the photograph (Figure 1) in the Photogrammetric Pioneers article about J. Victor Dallin (*PE&RS*, September 1984, page 1285) should read 25 September *1929*.